JOURNAL OF THE PHYSICAL SOCIETY OF JAPAN, Vol. 49, No. 3, SEPTEMBER, 1980

Raman Scattering and Infrared Reflectance in 2H-$MoSe_2$

Tomoyuki SEKINE, Mitsuru IZUMI, Tsuneo NAKASHIZU, Kunimitsu UCHINOKURA and Etsuyuki MATSUURA

Institute of Physics, The University of Tsukuba, Sakura-mura, Ibaraki 305

(Received March 17, 1980)

Raman scattering and infrared reflectance have been measured in 2H-$MoSe_2$. We observed all Raman-active modes, A_{1g}, E_{1g}, E^1_{2g} and E^2_{2g}, and two infrared-active modes, E^2_{1u} and A^2_{2u}. Intralayer force constants are estimated from the central force model. The bond between metal (Mo) and chalcogen (Se) predominates over the high-lying phonon frequencies with long wavelength. On the other hand, interlayer shear force constant is estimated from the frequency of E^2_{2g} mode, that is a rigid-layer mode, and is much smaller than the intralayer force constants. This fact, which is similar to that in other group VIB transition-metal dichalcogenides, reflects that the interlayer interaction is due to van der Waals force. The second-order Raman spectrum has been also observed and discussed.

§1. Introduction

Many investigations on the layered transition-metal dichalcogenides have been carried out for quasi-two dimensional properties.[1] These compounds have a layered structure of XMX, where M is a transition-metal atom from IVB, VB or VIB columns of the periodic table and X is one of the chalcogens, sulphur, selenium or tellurium. Strong intralayer bonds are primarily covalent in XMX layers, which are stacked with various types, and are weakly coupled with the adjacent layers by van der Waals force.

Electronic properties of these compounds have variations according to the species of transition metals. The transition-metal dichalcogenides composed of the group IVB and VIB transition-metal atoms are semiconductors or insulators, whereas the group VB compounds exhibit metallic properties.

The group VIB dichalcogenides such as MoS_2, $MoSe_2$, WS_2 and WSe_2 are composed of the trigonal prism structure and in the 2H stacking type the unit cell contains two prisms of adjacent layers. The symmetry of 2H-$MoSe_2$ belongs to the space group D^4_{6h} and there are 12 modes of lattice vibrations at the center of Brillouin zone. These are represented as[2]

$$A_{1g}+2A_{2u}+B_{1u}+2B_{2g}+E_{1g}+2E_{1u}+2E_{2g}+E_{2u}.$$

The A^1_{2u} and E^1_{1u} modes are acoustic, the A^2_{2u} and E^2_{1u} modes infrared active and the A_{1g}, E_{1g}, E^1_{2g} and E^2_{2g} modes Raman active. These modes are divided into six pairs. In each pair one mode is symmetric and the other antisymmetric with respect to the inversion around the center lying between the selenium atoms on both sides of the interlayer gap. They would be degenerate in the absence of interaction between layers. The small splitting of the frequencies of the pair reflects that the dispersion curves along c-axis are flat and in a word that this material has a two-dimensional character. Then it is interesting to study the lattice dynamics in the transition-metal dichalcogenides.

Raman scattering in 2H-$MoSe_2$ has been done by Agnihotri *et al.*[3,4] and by Smith *et al.*[5,6] Agnihotri *et al.* have obtained Raman spectra of MoS_2 and $MoTe_2$ in addition to $MoSe_2$ by exciting with He–Ne laser (6328 Å). Smith *et al.*[5,6] have measured all Raman-active and infrared-active phonons and in particular a rigid-layer mode at 92 cm^{-1}. They have emphasized that the interlayer interaction is not so weak as those previously reported in 2H-type compounds. This will be discussed in §4. The second-order Raman spectrum of 2H-$MoSe_2$ has not been reported. We are able to have informations about the two-phonon joint density of states from the second-order Raman spectrum.

Lucovsky *et al.*[7] have measured infrared reflectance spectrum on pressed pellets and observed the infrared-active modes of E_{1u}^2 and A_{2u}^2 at 288 cm^{-1} and 350 cm^{-1}. In a single crystal Uchida and Tanaka[8] have observed the reststrahlen band of the E_{1u}^2 mode, which is the only infrared-active mode when the polarization vector of incident light is perpendicular to the *c*-axis. Agnihotri *et al.*[4,9] also have observed the absorption spectrum of this mode at room temperature and at 77 K.

Many calculations of lattice dynamics have been carried out in the MoS_2 structure. Bromley[10] studied the lattice dynamics by means of the Born-von Karman model in the nearest-neighbour approximation for single layers, i.e. central force model. Wieting[11] has applied the simple linear-chain model to the long-wavelength phonons in MoS_2 and GaSe. In 2H-MoS_2 Wakabayashi *et al.*[12] investigated inelastic neutron scattering and analysed their data by a mixed model which includes valence forces between atoms within layer and axially symmetric forces between atoms in neighbouring layers. They calculated phonon dispersion curves and compared with their experimental data on high-symmetry lines in the Brillouin zone. Phonon density of states has also been calculated.

In the present work we will report the first- and the second-order Raman scattering and the infrared reflectance spectra in 2H-$MoSe_2$ and study the lattice dynamics.

§2. Experimental Techniques

Raman scattering was measured on single crystals of 2H-$MoSe_2$, while infrared reflectance measurements were carried out both on single crystals and on powders. Single crystals were grown by sublimation method from prereacted stoichiometric powders. Single crystals are thin flat hexagonal plates with the area 0.5 mm^2 to 15 mm^2.

Measurements of Raman scattering were performed by the reflection method. In reflection Raman scattering, the condition of the surface strongly affects the intensity of Rayleigh scattering. As-grown and cleaved surfaces offer very good conditions for surface reflection Raman scattering. Power of an Argon ion laser is reduced as weak as possible in order to keep a good surface on the sample. When the exciting light is polarized in the plane of the incidence, the angle of incidence was set up so as to maximize the power transmitted into the sample. This incident angle is a Brewster's angle and about 78° in this case. However, since the refractive index of 2H-$MoSe_2$ is large around 5000 Å,[13] the wave vector of the incident light is approximately perpendicular to the surface inside the crystal. The Raman spectra were obtained at room temperature and at liquid N_2 temperature using a Spex 1401 double monochromator with third monochromator, a thermoelectrically cooled photomultiplier and a photon counting detection. Infrared reflectance measurements were carried out with a Beckman IR-720M Fourier spectrophotometer which covers the spectral region from 50 cm^{-1} to 1000 cm^{-1}.

§3. Experimental Results

2H-$MoSe_2$ has a symmetry of the space group D_{6h}^4 and has 12 phonon modes at Brillouin zone center. Raman-active phonons are four modes, A_{1g}, E_{1g}, E_{2g}^1 and E_{2g}^2, whose atomic motions are shown in Table I of ref. 3. The E_{2g}^2 mode is called "rigid-layer" or "quasi-acoustic" mode. With X=[100], Y=[010] and Z=[001], Raman tensors are written as follows,[14]

$$A_{1g}: \begin{pmatrix} a & & \\ & a & \\ & & b \end{pmatrix},$$

$$E_{1g}: \begin{pmatrix} & c & \\ c & & \\ & & \end{pmatrix}, \quad \begin{pmatrix} & & -c \\ & & \\ -c & & \end{pmatrix},$$

and

$$E_{2g}: \begin{pmatrix} & d & \\ d & & \\ & & \end{pmatrix}, \quad \begin{pmatrix} d & & \\ & -d & \\ & & \end{pmatrix}. \qquad (1)$$

Figure 1 shows the Raman spectra from 30 cm^{-1} to 700 cm^{-1} excited with 5145 Å line of Argon ion laser at room temperature. They are obtained with p- and s-polarizations of the incident laser light, in which the electric fields are parallel and perpendicular to the plane of incidence, respectively. In Raman spectrum excited with p-polarized incident light, two sharp peaks are observed at 168 cm^{-1} and 242 cm^{-1}, which are first-order Raman peaks. But the peak at 168 cm^{-1} disappears in the spectrum with s-polarized incident light.

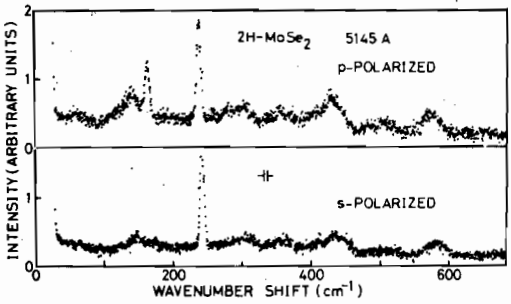

Fig. 1. Raman spectra of 2H-$MoSe_2$ at room temperature with s- and p-polarized incident light. They are excited with 5145 Å laser line.

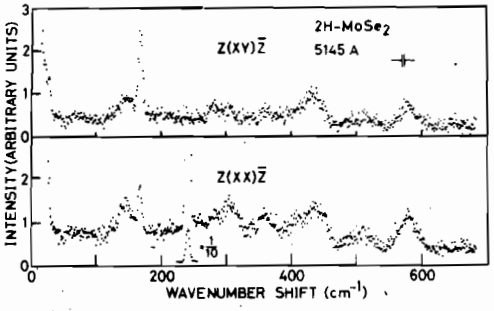

Fig. 2. Polarization characteristic of Raman scattering of 2H-$MoSe_2$ with p-polarized incident light. X, Y and Z are along [100], [010] and [001] crystallographic axes. These spectra are excited with 5145 Å laser line at room temperature.

Polarization characteristic excited with p-polarized incident light is shown in Fig. 2. The sharp peak at 242 cm^{-1} appears only in the $Z(XX)\bar{Z}$ polarization configuration, while the intensity of the peak at 168 cm^{-1} in the $Z(XY)\bar{Z}$ configuration is twice that in the $Z(XX)\bar{Z}$ configuration. In the $Z(XX)\bar{Z}$ configuration, the A_{1g} mode is allowed but not in the $Z(XY)\bar{Z}$ configuration from eq. (1). Therefore the peak at 242 cm^{-1} is an A_{1g} mode. The remarkable feature for the peak at 168 cm^{-1} is that it disappears completely in the spectrum with s-polarized incident light. In our experimental configuration (see §2), the angle between the wave vector of the scattered light and the Z axis is about 2° inside the crystal. It may be good for us to consider that the scattered light goes along Z axis inside the crystal. On the other hand, the wave vector of the incident light inside the crystal is about 11° from the Z axis, where we neglect anisotropy in the refractive index because we do not have

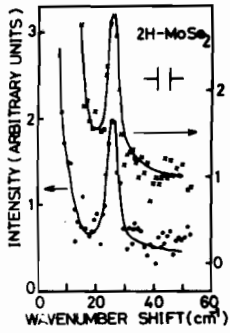

Fig. 3. Raman spectra of 2H-$MoSe_2$ in the $Z(XX)\bar{Z}$ (×) and $Z(XY)\bar{Z}$ (●) configurations in low-frequency region with p-polarized incident light. They are obtained with high resolution by using 5145 Å laser line at room temperature.

a knowledge of the refractive index parallel to the *c*-axis. Therefore, the electric field of the incident light has some Z components only in the spectrum with the p-polarized incident light. The appearance of the peak at 168 cm^{-1} in the spectrum with p-polarized incident light is attributed to depolarization arising from the deviation from a 90° geometry. Then we assign it to E_{1g} mode. We also observed a sharp peak at low frequency by measuring with better resolution, as shown in Fig. 3. The energy of this peak is 25.4 cm^{-1} and has nearly equal intensities in the $Z(XX)\bar{Z}$ and $Z(XY)\bar{Z}$ polarization configurations. Since this peak has a property of E_{2g} symmetry and low frequency, it is a rigid-layer mode. In this mode the layers move very nearly as rigid units and the phase of the motion of one layer is opposite to that of the other. This mode is observed in other transition-metal dichalcogenides by Raman scattering, for example 2H-MoS_2,[15,16] 2H-WSe_2,[17,18] 2H-$TaSe_2$,[19] 2H-$NbSe_2$,[20,21] and 2H-WS_2.[22] We did not observe a Raman-active E^1_{2g} mode with 5145 Å excitation. But, as the wavelength of the laser line becomes shorter, a new sharp peak appears at 286 cm^{-1} as shown in Fig. 4. And we conclude that it is the E^1_{2g} mode from polarization measurement in Fig. 5. In absorption and reflection spectra of 2H-$MoSe_2$,[13,23] A, B, A′ and B′ exciton peaks and many peaks due to the band-to-band transition appear above 1.1 eV. Figure 4 shows that the Raman intensity of the E^1_{2g} mode is enhanced by the C band-to-band transition at about 2.8 eV.[23] This resonant effect of the E^1_{2g} and A_{1g} modes

will be reported soon in detail. In Figs. 1 and 2, several broad bands are the second-order Raman spectra.

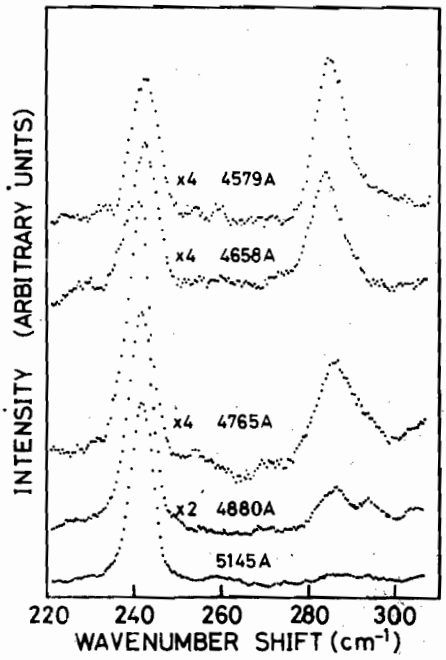

Fig. 4. Raman spectra of 2H-$MoSe_2$ at room temperature in the region from 220 cm^{-1} to 305 cm^{-1} for various frequencies of p-polarized incident light.

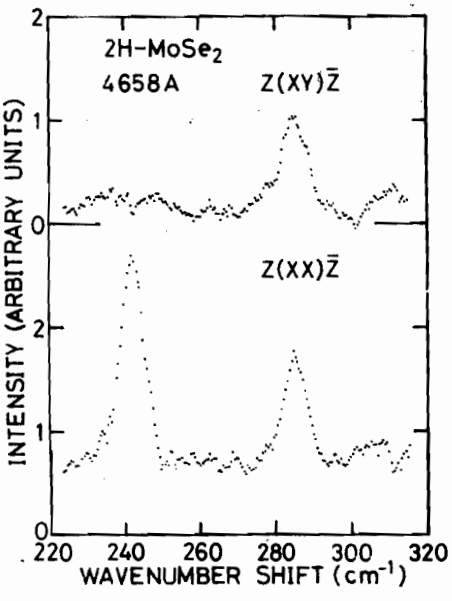

Fig. 5. Polarization characteristic of Raman scattering of 2H-$MoSe_2$ excited with p-polarized 4658 Å laser line.

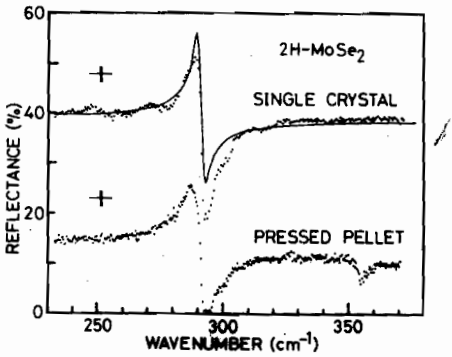

Fig. 6. Infrared reflectance at room temperature in single crystal and pressed pellet. The solid curve is calculated from the single damped classical oscillator model by using $\varepsilon_0=18.7$, $\varepsilon_\infty=18.4$, $\Gamma=2.8\ cm^{-1}$ and $\omega_{TO}=289\ cm^{-1}$.

Infrared reflectance spectra of a single crystal and a pressed pellet at room temperature are shown in Fig. 6. The reststrahlen band at 289 cm^{-1} is observed either in the single crystal, in which the electric field vector is perpendicular to the c-axis, or in the pressed pellet, in which the direction of the crystal axes are randomly distributed to the electric field vector of the light. On the other hand the band at 352 cm^{-1} is observed only in the pressed pellet. We obtained the same results in powders planted with the vacuum grease on a sample holder as those in the pressed pellet. The A_{2u}^2 and E_{1u}^2 modes are infrared allowed for the electric field vector parallel and perpendicular to the c-axis, respectively. Therefore we determine that the band at 289 cm^{-1} is assigned to the E_{1u}^2 mode and the band at 352 cm^{-1} to the A_{2u}^2 mode. The reflectance spectrum in the single crystal is fitted with the curve computed by using the single damped classical oscillator model, which is shown by the solid curve in Fig. 6. In the computation, we used the values, $\varepsilon_0=18.7$, $\varepsilon_\infty=18.4$, $\Gamma=2.8\ cm^{-1}$ and $\omega_{TO}=289\ cm^{-1}$. From the Lyddane-Sachs-Teller relation we determine that LO phonon frequency is 292 cm^{-1}. The splitting of the LO-TO phonon frequencies is small and this fact shows that the macroscopic effective charge e_T^* is very small in this crystal. The frequency of the Raman-active E_{2g}^1 mode is 286 cm^{-1} and is very close to that of the conjugate E_{1u}^2 mode.

§4. Discussion

Several workers have studied infrared

spectroscopy and Raman scattering in 2H-$MoSe_2$ and their results are shown in Table I in addition to our data. Raman spectrum of Agnihotri *et al.*[3] is not similar to ours, shown in Fig. 1, and their spectrum in 2H-MoS_2 also differs completely from those of Wieting and Verble[24] and Chen and Wang.[16] Therefore the results of Agnihotri *et al.* seem to be incorrect. These may be probably due to the observation of plasma lines of the laser. Smith *et al.*[5,6] have observed all Raman-active and infrared-active modes. But their result is different from ours in Raman scattering except the A_{1g} mode. They have not reported their results in detail. However, the frequency of the rigid-layer mode (E^2_{2g}) is too high. Considering the weak coupling between the layers in the transition-metal dichalcogenides, the rigid-layer mode must have low frequency, and our result is reasonable in comparison with the other transition-metal dichalcogenides. Because the E^1_{2g} and E^2_{1u} modes are conjugate to each other, the frequencies have nearly the same values. The splitting between the frequencies of the E^1_{2g} and E^2_{1u} modes obtained by Smith *et al.*, 16 cm^{-1}, is too large. They also observed the E_{1g} mode at 150 cm^{-1}, where a broad peak appears in our spectra. This comes from the second-order Raman spectrum due to difference combination as mentioned below. Therefore they may have misinterpreted in its assignment. For an infrared-active E^2_{1u} mode, Agnihotri *et al.*[4,9] have measured absorption spectra at room temperature and at 77 K in single crystal and Uchida and Tanaka[8] also have obtained the reflectance spectrum. They analysed their spectrum by a single damped oscillator model. This analysis was also done by us as shown in Fig. 6. The values of ε_0, ε_∞, Γ and ω_{TO} used in the analysis are shown in Table II in addition to the oscillator strength S, the frequency of the longitudinal optical phonon ω_{LO} and the macroscopic effective charge e^*_T, which are calculated from ε_0, ε_∞ and ω_{TO}. The results obtained by Agnihotri *et al.* are different from ours and Uchida and Tanaka's. The macroscopic effective charge obtained by us is nearly equal to those of other group VIB transition-metal dichalcogenides.[8] The value of Agnihotri *et al.* is as large as those of the group IVB compounds,[8] and therefore it may be incorrect. Our result, that the e^*_T is very small, indicates that the covalency in chemical bonding is much stronger than the ionicity in 2H-$MoSe_2$, though the e^*_T does not directly mean the ionicity.[25,26]

In the lattice dynamics of the layered compounds like the transition-metal dichalcogenides, it is good to assume that a layer is an isolated molecule and the atoms in it are connected with each other by strong springs, and the molecules are coupled by soft springs. Therefore we are able to understand the lattice dynamics of this compounds by neglecting the interlayer forces except the rigid-layer modes. In practice, from a simple model[27] in layered

Table I. Optical-phonon frequencies (cm^{-1}) of 2H-$MoSe_2$ observed by several workers.

	E^2_{2g}	E^2_{1u}	E^1_{2g}	E_{2u}	E_{1g}	B^2_{2g}	A^2_{2u}	B^1_{2g}	B_{1u}	A_{1g}
Agnihotri[a] *et al.*	112	277	285		217					361
Lucovsky[b] *et al.*		288					350			
Smith[c] *et al.*	92	286	302		150		352			244
Uchida[d] *et al.*		286.9								
Ours	25.4	289	286		168		352			242

[a] Refs. 3, 4 and 9. [b] Ref. 7. [c] Refs. 5 and 6. [d] Ref. 8.

Table II. Dielectric dispersion parameters and constants for the E^2_{1u} mode of 2H-$MoSe_2$ single crystal.

	ε_0	ε_∞	S	Γ (cm^{-1})	ω_{TO} (cm^{-1})	ω_{LO} (cm^{-1})	e^*_T/e
Agnihotri[a] *et al.*	16.81	10.24	6.57	—	277	355	6.00
Uchida[b] *et al.*	18.5	18.0	0.5	2.2	286.9	290.9	1.7
Ours	18.7	18.4	0.3	2.8	289	292	1.33

[a] Refs. 4 and 9. [b] Ref. 8.

crystals with two layers per unit cell, the Davydov splitting of an intralayer mode is written by $\omega_1^2/(2\omega_0)$, where ω_1 is a frequency of the rigid-layer mode, which comes from the interlayer force constant, and ω_0 is a frequency of an optical phonon. In 2H-$MoSe_2$, this splitting is calculated to be about 2 cm^{-1} and therefore neglected. Bromley[10] used the central force model to calculate the lattice vibrations of the MoS_2 structure in a single layer under the assumption of nearest neighbour interactions. When we do not assume the ideal coordination geometry ($a=c$), the frequencies of the intralayer optical phonons at Brillouin zone center are given as follows,

$$\omega^2(E_{2g}^1)\simeq\omega^2(E_{1u}^2)=(3/\mu)\gamma\xi',$$
$$\omega^2(E_{1g})\simeq\omega^2(E_{2u})=(3/(2m_2))\gamma\xi',$$
$$\omega^2(B_{2g}^1)\simeq\omega^2(A_{2u}^2)=(6/\mu)\gamma\xi,$$
$$\omega^2(A_{1g})\simeq\omega^2(B_{1u})=(3/m_2)(\gamma\xi+(2/3)\beta), \quad (2)$$

where

$$\xi=\frac{3c^2}{4a^2+3c^2}, \quad \xi'=1-\xi, \quad \frac{1}{\mu}=\frac{1}{m_1}+\frac{1}{2m_2},$$

and m_1, m_2 are the masses of metal and chalcogen atoms, respectively, a is the atomic distance between metal and metal or chalcogen and chalcogen in the X-Y plane and c is the thickness of the layer. β and γ are the force constants of chalcogen-chalcogen bond along Z direction and metal-chalcogen bond, respectively. Recently the same result was obtained by Maiti and Ghosh.[28] The low-lying frequencies of the rigid-layer modes provide quantitative information about the interlayer forces. According to **Verble *et al.*,**[15] the frequencies of these phonons are given by

$$\omega^2(E_{2g}^2)=4K_s/(m_1+2m_2),$$

and

$$\omega^2(B_{2g}^2)=4K_c/(m_1+2m_2), \quad (3)$$

where K_s and K_c are the interlayer shear and compressional force constants, respectively. We evaluated the optimum magnitudes of the force constants from eqs. (2) and (3). Table III shows the results for 2H-MoS_2, 2H-WS_2 and 2H-WSe_2 in addition to 2H-$MoSe_2$. The calculated frequencies are in reasonable agreement with experimental data. Because the force constants have nearly the same mag-

Table III. Phonon frequencies and force constants in the group VIB transition-metal dichalcogenides.

	$MoSe_2$	MoS_2	WSe_2	WS_2
a (A)	3.288[a]	3.160[a]	3.286[b]	3.154[b]
c (A)	3.23[a]	3.19[a]	3.287[b]	3.157[b]
$N_A m_1$[c] (g)	95.95	95.95	183.86	183.86
$N_A m_2$[c] (g)	78.96	32.066	78.96	32.066
β ($\times 10^4$ dyn/cm)	3.19	3.42	3.33	3.62
γ ($\times 10^4$ dyn/cm)	16.6	19.0	17.6	20.7
K_s ($\times 10^4$ dyn/cm)	0.242	0.242	0.283	0.275
K_c ($\times 10^4$ dyn/cm)	—	0.739	—	—

	obs. (cm^{-1})	cal. (cm^{-1})	obs. (cm^{-1})	cal. (cm^{-1})	obs. (cm^{-1})	cal. (cm^{-1})	obs. (cm^{-1})	cal. (cm^{-1})
E_{1u}^1	0	0	0	0	0	0	0	0
E_{2g}^2	25.4	25.4	32.0[d]	32.0	23.7	23.7	27.4	27.4
E_{1u}^2	289	286	384.3[e]	377	247.4[d]	246	354.5[e]	356
E_{2g}^1	286	286	383.0[d]	377	247	246	357	356
E_{2u}	—	176	—	292	—	180	—	306
E_{1g}	168	176	286.0[d]	292	186	180	—	306
A_{2u}^1	0	0	0	0	0	0	0	0
B_{2g}^2	—	—	56.0[f]	56.0	—	—	—	—
A_{2u}^2	352	344	470[g]	467	305[h]	301	435[h]	436
B_{2g}^1	—	344	—	467	—	301	—	436
B_{1u}	—	242	—	408	--	251	—	423
A_{1g}	242	242	408.3[e]	408	251	251	423	423

[a] Ref. 1. [b] F. R. Gamble: J. Solid State Chem. 9 (1974) 358. [c] N_A is the Avogadro number. [d] Ref. 16. [e] Ref. 8. [f] Ref. 12. [g] Ref. 24. [h] Ref. 7. Other data are ours.

nitudes in β, γ and K_s in the group VIB compounds, the phonon frequencies at Brillouin zone center mainly depend on the masses of the metal and the chalcogen. The metal-chalcogen bonding γ is much stronger than the chalcogen-chalcogen bonding β. This result coincides with the fact that the covalent bond is caused by the *s-p* mixed orbital from the *s* electron in metal and the *p* electron in chalcogen, and the group VIB compounds have a covalent character of bonding electrons rather than a metallic nature. In practice the ratios β/γ for the group VIB compounds are much smaller than those for 2H-$NbSe_2$ with metallic nature[20] and for 3R-NbS_2 with semimetallic nature.[29] The interlayer shear force constant is much smaller than the intralayer force constants, which is consistent with the fact that the interlayer force constant originates from van der Waals force. The rigid-layer mode B_{2g}^2 is neither Raman active nor infrared active. Therefore we can not estimate the interlayer compressional force constant K_c except in 2H-MoS_2, in which Wakabayashi *et al.*[12] have observed the B_{2g}^2 phonon by neutron diffraction.

The second-order Raman spectra of 2H-$MoSe_2$ have been observed in the range from 40 cm^{-1} to 650 cm^{-1} at room temperature and at liquid N_2 temperature as shown in Fig. 7. As is well known, the second-order Raman spectrum reflects the two-phonon joint density of states and then we are able to get informations about phonons not only at Brillouin zone center but also in whole Brillouin zone by critical-point analysis. In the group VIB compounds the second-order Raman spectra of

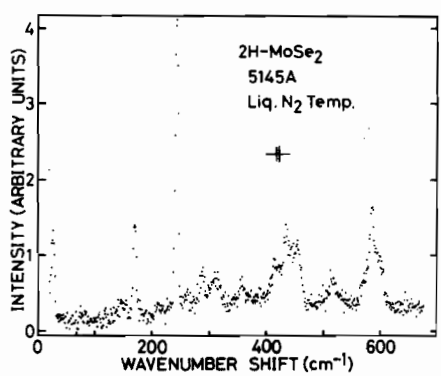

Fig. 7. Raman spectrum at liquid N_2 temperature with p-polarized incident light of 5145 Å.

2H-MoS_2[16] and 2H-WSe_2[18] were obtained, and they resemble each other. But the second-order Raman spectrum of 2H-$MoSe_2$ is very different from those of 2H-MoS_2 and 2H-WSe_2. Wakabayashi *et al.*[12] have measured phonon frequencies along the principal symmetry directions in the Brillouin zone by inelastic neutron scattering techniques in 2H-MoS_2. We analysed their results by the central force model, where we divide chalcogen-chalcogen force constants into that in X-Y plane and that along Z direction against Bromley's assumption. The analysis is in good agreement with neutron data in phonon frequencies except in the transverse acoustic phonon along [100] direction.[30] As described above, the group VIB transition-metal dichalcogenides have nearly the same force constants. Mass ratio of the metal and chalcogen atoms in 2H-MoS_2 is close to that in 2H-WSe_2, too. Therefore, phonon dispersion curves and second-order Raman spectra of 2H-MoS_2 and 2H-WSe_2 resemble each other. Mass ratio of 2H-$MoSe_2$, however, is much smaller than those of 2H-MoS_2 and 2H-WSe_2. This fact explains the difference of the second-order Raman spectrum of 2H-$MoSe_2$ from those of 2H-MoS_2 and 2H-WSe_2.

The two-dimensional materials, with relatively flat phonon dispersions, show distinguished natures on the density of states and the second-order Raman spectrum. The critical points in the dispersions play an important role in the second order Raman spectrum and have three types of singularities as shown in Fig. 2 of ref. 31. In particular the M_1 singularity has a logarithmic divergence.[32,33] In order to observe these features more clearly, we measured the second-order Raman spectrum at liquid N_2 temperature. Contrary to the second-order Raman spectra of three-dimensional semiconductors, for example Ge[34] and Si[35,36] the second-order spectrum of 2H-$MoSe_2$ has narrower peaks and sharper slopes. This must be due to the two-dimensional nature of the material. The peak at 145 cm^{-1} becomes extremely weak at liquid N_2 temperature in comparison with that at room temperature. Therefore this structure is a two-phonon difference process,[16] which creates a phonon and absorbs another, and several structures above 300 cm^{-1} are the two-phonon overtone

or combination processes. Though we have not detailed knowledge of the dispersion curves in the Brillouin zone, we can tentatively identify the sharp peak at 588 cm^{-1} as due to the overtone of E^1_{2g} and E^2_{1u} among the many features in the spectrum.

§5. Summary

The first-order and the second-order Raman and the infrared reflectance spectra have been measured in layered compounds 2H-$MoSe_2$. All Raman-active and infrared-active modes are observed and assigned by polarization analyses in Raman scattering and infrared reflectance. The Raman-active phonon E^1_{2g} was observed in the resonance region of the incident light. By application of the central force model we conclude that the force constant between the metal and chalcogen atoms, γ, is predominant in $q=0$ phonon frequencies. The interlayer shear force constant was estimated from the frequency of the rigid-layer mode E^2_{2g} and is much smaller than the intralayer force constants. This fact tells us that the interlayer bond is due to van der Waals force. The results were compared with those of other group VIB transition-metal dichalcogenides and we have shown that they have nearly the same force constants and therefore the differences of phonon frequencies depend strongly on the masses of metal and chalcogen atoms. In the second-order Raman spectrum at liquid N_2 temperature, many structures show two-dimensional features. Also infrared spectrum was analysed by means of the single classical oscillator model and the macroscopic effective charge was calculated and found to be small. This fact reflects that the covalency is very strong in this materials.

After the completion of this work, we became aware of the paper reported by Wieting, Grisel and Levy.[37] Their experimental results are similar to ours, but we obtained more distinct result in the resonance effect of the E^1_{2g} phonon and complete second-order Raman spectra at room and liquid N_2 temperatures. In lattice dynamics our analysis is different from theirs. They applied a linear-chain model[6,11] and calculated the Raman and infrared frequencies by mass-scaling the data on MoS_2.

References

1) J. A. Wilson and A. D. Yoffe: Adv. Phys. **18** (1969) 193.
2) J. L. Verble and T. J. Wieting: Phys. Rev. Lett. **25** (1970) 362.
3) O. P. Agnihotri, H. K. Sehgal and A. K. Garg: Solid State Commun. **12** (1973) 135.
4) O. P. Agnihotri and H. K. Sehgal: Phil. Mag. **26** (1972) 753.
5) J. E. Smith, Jr., J. B. Torrance and M. W. Shafer: Bull. Am. Phys. Soc. **18** (1973) 396.
6) T. J. Wieting and J. L. Verble: *Electrons and Phonons in Layered Crystal Structures* ed. T. J. Wieting and M. Schlüter (Reidel, Dordrecht, 1979) p. 321.
7) G. Lucovsky, R. M. White, J. A. Benda and J. F. Revelli: Phys. Rev. B7 (1973) 3859.
8) S. Uchida and S. Tanaka: J. Phys. Soc. Jpn. **45** (1978) 153.
9) A. K. Garg, H. K. Sehgal and O. P. Agnihotri: Solid State Commun. **12** (1973) 1261.
10) R. A. Bromley: Phil. Mag. **23** (1971) 1417.
11) T. J. Wieting: Solid State Commun. **12** (1973) 931.
12) N. Wakabayashi, H. G. Smith and R. M. Nicklow: Bull. Am. Phys. Soc. II, **17** (1972) 297; Phys. Rev. B12 (1975) 659.
13) B. L. Evans and R. A. Hazelwood: Phys. Status Solidi (a) **4** (1971) 181.
14) R. Loudon: Adv. Phys. **13** (1964) 423.
15) J. L. Verble, T. J. Wieting and P. R. Reed: Solid State Commun. **11** (1972) 941.
16) J. M. Chen and C. S. Wang: Solid State Commun. **14** (1974) 4286.
17) D. G. Mead and J. C. Irwin: Can. J. Phys. **55** (1977) 379.
18) T. Sekine, T. Nakashizu, K. Uchinokura and E. Matsuura: in preparation.
19) E. F. Steigmeier, G. Harbéke, H. Auderset and F. J. DiSalvo: Solid State Commun. **20** (1976) 667.
20) C. S. Wang and J. M. Chen: Solid State Commun. **14** (1974) 1145.
21) J. R. Duffey, R. D. Kirby and R. V. Coleman: *Light Scattering in Solids*, ed. M. Balkanski, R. C. C. Leite and S. P. S. Porto (Flammarion, Paris, 1976) p. 383.
22) T. Sekine, T. Nakashizu, K. Toyoda, K. Uchinokura and E. Matsuura: to be published in Solid State Commun.
23) A. R. Beal, J. C. Knight and W. Y. Liang: J. Phys. C5 (1972) 3540.
24) T. J. Wieting and J. L. Verble: Phys. Rev. B3 (1971) 4286.
25) E. Burstein, A. Pinczuk and R. F. Wallis: *The Physics of Semimetals and Narrow-Gap Semiconductors*, ed. D. L. Carter and R. T. Bate (Pergamon, New York, 1970) p. 251.
26) G. Lucovsky, R. M. Martin and E. Burstein: Phys. Rev. B4 (1971) 1367.
27) R. Zallen: *Proc. 12th Int. Conf. Phys. of Semiconductors*, ed. M. H. Kuhn (B. G. Teubner, Stut-

tgart, 1974) p. 621.
28) C. R. Maiti and R. N. Ghosh: J. Phys. C**11** (1978) 2475.
29) S. Onari, T. Arai, R. Aoki and S. Nakamura: Solid State Commun. **31** (1979) 577.
30) T. Sekine, K. Uchinokura and E. Matsuura: unpublished.
31) B. L. Evans: *Optical and Electrical Properties*, ed. P. A. Lee (Reidel, Dordrecht, 1976) p. 1.
32) W. A. Bowers and H. B. Rosenstock: J. Chem. Phys. **18** (1950) 1056.
33) J. L. Hwang: Phys. Rev. **99** (1955) 1098.
34) B. A. Weinstein and M. Cardona: Phys. Rev. B**6** (1973) 2545.
35) P. A. Temple and C. E. Hathaway: Phys. Rev. B**7** (1973) 3685.
36) K. Uchinokura, T. Sekine and E. Matsuura: J. Phys. Chem. Solids **35** (1974) 171.
37) T. J. Wieting, A. Grisel and F. Lévy: Physica **99**B (1980) 337.